SIGNAL ENHANCEMENT IN DISPERSE SOLUTIONS FOR THE ANALYSIS OF BIOMEDICAL SAMPLES BY PHOTOTHERMAL SPECTROSCOPY

Authors:

M.A. Proskurnin, D.S. Volkov, E.S. Ryndina, D.A. Nedosekin, V.P. Zharov

Corresponding author: M.A. Proskurnin

e-mail: proskurnin@gmail.com

Signal Enhancement in Disperse Solutions for the Analysis of Biomedical Samples by Photothermal Spectroscopy

M.A. Proskurnin[1], D.S. Volkov[1], E.S. Ryndina[1], D.A. Nedosekin[2], V.P. Zharov[2]

[1]Analytical Chemistry Division, Chemistry Department, Lomonosov Moscow State University, Moscow, 119991, Russia

[2]Philips Classic Laser Laboratories, University of Arkansas for Medical Sciences, Little Rock, Arkansas, 72205, USA

Abstract

Photothermal lens spectrometry not only shows high sensitivity of colored heme protein determination, but also provides a change in the sensitivity compared to the theoretical values due to changes in the heat transfer in dispersed media. This can be used for estimating the size of disperse particles exemplified by hemoglobin cyanide, photothermal examination of the state of existence of hemoglobin in highly saline solutions by changes in photothermal properties upon dissociation of hemoglobin tetramers into dimers and monomers. The example of determination of contrast agents (dyes) in blood as the versification of the platform of photoacoustic/photothermal measurement of circulating blood volume is shown.

Introduction

Photothermal spectroscopy develops in many directions, and since the 1980s, it had been used in various analytical applications, which include highly sensitive photometric measurements and versatile detection schemes in liquid chromatography and capillary electrophoresis [1]. Recently, much attention is paid to the applications of photothermal spectroscopy in microfluidic systems (chemical microchips or μ-TAS), which begin to play a key role in analytical chemistry [2]. However widespread these well-known areas of photothermal applications are, the potentialities of photothermics in analytical chemistry and chemical analysis are even wider.

In this study, we use PTS measurements of protein heme suspensions at high and trace level of constituents in various media (aqueous solutions). Such disperse media are characterized by a multitude of conversion mechanisms, with the main feature of their simultaneous and competing character. Moreover, the existing of particles with constantly changing configuration provides a random constituent of the signal. These features were observed as functions of dynamic (response profile) and statistic (amplitude fluctuation) parameters of PTS signals and disperse-phase parameters.

Materials and Methods

Photothermal setups

The design of the optical scheme of continuous-wave (cw) mode PT-lens spectrometer was based on previously made optimization [3]. The schematic (Fig. 1) is based on recording an excitation (IDLS5, Polyus, Moscow; wavelengths 532, 610, 635, 660 and 690 nm; waist diameter, 59.8 ± 0.5 μm; power range 1–20 mW) diode-laser-induced refractive heterogeneity (thermal-lens effect) causing defocusing of a collinear diode laser probe beam (wavelength, 808 nm; waist diameter, 25.0 ± 0.2 μm; (attenuated) power, 1 mW) and hence a reduction in the probe beam intensity at its centre as detected by a far-field photodiode (sample-to-detector distance 180 cm) supplied with a stained-glass broadband-range (610–640 nm) bandpass filter and a 2-mm-diameter pinhole (Fig. 1). Other parameters are summarized in Table 1.

The synchronization of the measurements is implemented by in-house written software. The PT spectrometer has a linear dynamic range of the signal of four orders of magnitude (the corresponding range of absorption coefficients for 10 mm optical pathways is 1×10^{-6} to 2×10^{-2} cm^{-1}) and response time of 0.005–2 s (depending on the selected measurement parameters, namely, on the data throughput rate and time, the number of points to be averaged, etc.). The spectrometer implements a secondary channel (for gathering scattering signal, if present). The probe beam was reflected by a dichroic mirror; the residual excitation beam was removed with a stained-glass bandpass filter and after a 2-mm pinhole appeared at the primary PT detector. If the photometric or PT channel is not needed, the corresponding detector is switched off. The scattering at the excitation wavelengths was collected with the secondary photodiode near the flowing cell and used to correct the absorbance value, see below.

Flow manifold for in vitro measurements

The flow manifold consisted of a circular flow system pumped with a Watson–Marlow 501U peristaltic pump (UK), a cylindrical flow cell
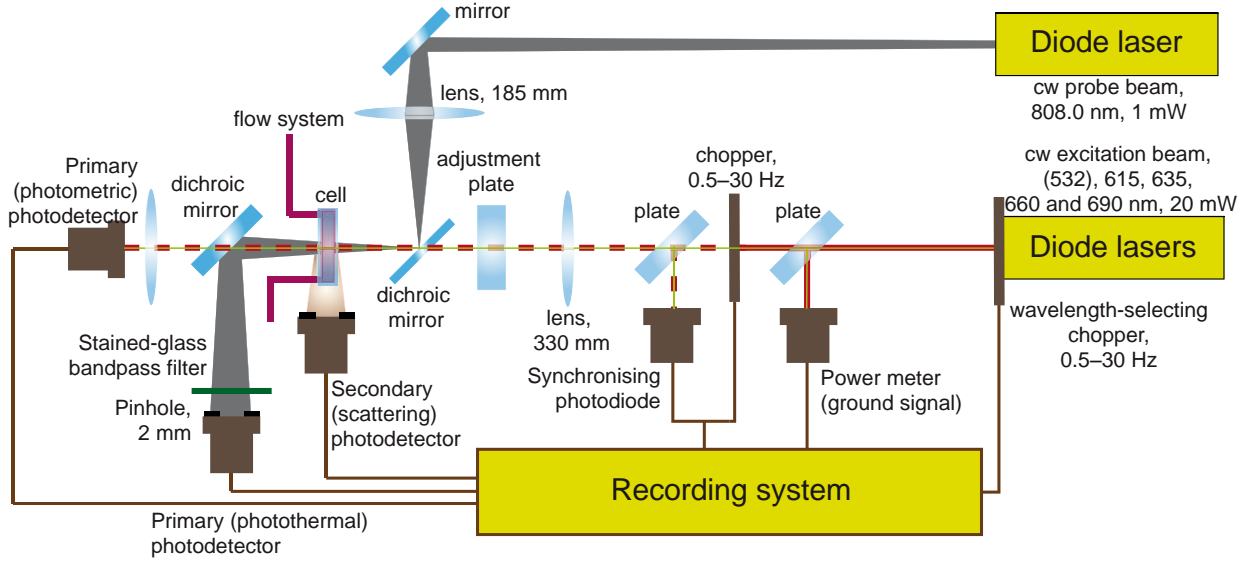
Fig. 1. Schematics of the dual-beam flow thermal-lens spectrometer-photometer

(l = 15 mm; 16 cm^3) and a changeable (volume-adjusting) vessel (volume 0.25 to 6 L).

All the tubing parts were from a KDM blood-transfusion system (KD Medical GmbH, Germany; length 90 cm, i.d. 0.3 cm). The system was filled with doubly distilled water, PBS, or stabilized rat blood. The dye was injected through an injected valve before the measurement cell to emulate the injection of the target dye in *in vivo* tests. The flow rate was kept at 35 ± 1 mL/min (linear velocity 2 cm/s). After each measurement, the working liquid was drained to waste and washed with distilled water through a secondary injection valve. The measurements were made using the PT setup or with a Shimadzu UV Mini 1240 spectrophotometer, Japan (optical absorbance measurements).

Data Treatment

The instrumental signal during an excitation on–off cycle (chopper cycle) is ($\vartheta(t)$),

$$\vartheta(t) = \frac{I_p(0) - I_p(t)}{I_p(t)}, \qquad (1)$$

where $I(0)$ and $I(t)$ are intensities of the probe beam in the centre of a detector during the heating part of the chopper cycle. According to the diffraction theory of thermal lensing [4-6], the interrelation between the absorption-based (analytical) signal θ (see below, (5)) and the instrumental ϑ signal is

$$\vartheta(t) = (1 - B(t)\theta)^{-2} - 1, \qquad (2)$$

where $B(t)$ is the time-dependent geometry-configuration constant of thermal-lens spectrometer [7].

$$B(t) = \frac{1}{2}\tan^{-1}\left(\frac{2mV}{\left[(1+2m)^2 + V^2\right](t_c/2t) + 1 + 2m + V^2}\right) \qquad (3)$$

Table 1. Experimental parameters for the optimization of the optical-scheme configuration of the dual-beam PT-lens spectrometer, T = 293K

Excitation laser	λ_e	532, 610, 635, 660 and 690 nm
	Focusing lens focal length, f_e	300 mm
	Rayleigh range, z_{ce}	25–32 mm
	laser power at cell(s)	1–20 mW
	spot size at the waist, $2\omega_{0e}$	60 µm
Probe laser	λ_p	808 nm
	Focusing lens focal length, f_p	185 mm
	Rayleigh range, z_{cp}	7.1 mm
	laser power at cell(s)	1 mW
	spot size at the waist, $2\omega_{0p}$	38 µm
Other constants	Optical path length of cells	10.00 ± 0.05 mm
	E_0, Eq.	0.12 mW^{-1}
	Cell to detector distance	95 cm

Here m is the ratio of cross-section areas of the probe and excitation beams at the sample, and V is the relative distance from the excitation waist to the sample, and

$$t_c = \omega_{0e}^2 \rho C_p / 4k \qquad (4)$$

is the characteristic time of the thermal lens. The meanings of other parameters are summed up in Table 1. Analytical signals is given by

$$\theta_{TLS} = 2.303\varepsilon l c E_0 P_e = 2.303 A E_0 P_e, \qquad (5)$$

where ε is apparent molar absorptivity; l is optical pathlength of the medium; c is molar concentration;

P_e is the excitation power; A is absorbance; and E_0 is the enhancement factor of thermal lensing:

$$E_0 = -\frac{dn/dT}{\lambda_p k}. \qquad (6)$$

Here, λ_p is the probe wavelength; dn/dT is the temperature gradient of the refractive index, and k is the thermal conductivity.

A theoretical description for two-beam photothermal-lens detection coupled to optoacoustic detection and pulsed laser modes for solutions with multi-point light-absorbing entities: nanoparticles (1 – 300 nm), organelles [mitochondria] (0.5 – 3 μm), cells (5 – 20 μm), bacteria (5 – 20 μm) and proteins (0.1 – 3 μm) [8-16]. The theory makes it possible to estimate the irregularities of temperature and refractive-index profiles for a discrete number of particles in a laser beam and a change the concentration and particles size parameters for the system.

Each determination was characterized by the limit of detection (LOD) calculated as the analyte concentration that produces a thermal lens signal which is three times greater than the standard deviation of the blank solution (3σ-criterion). The limit of quantification (LOQ) calculated from the $RSD_{rlc} = f(c)$ curves is the analyte concentration that produces estimates having a relative standard deviation of 10% (10σ-criterion)

The minimum detectable linear absorption coefficients for PT and photometric (PM) measurements were calculated according to the equations previously deduced from the theory of these two methods for the conditions of shot noise determining the measurement precision [17]

$$\alpha_{min}^{PT} = \sqrt{\frac{2h\nu_p}{\eta P_p}} \Delta f \frac{B_\infty \omega_{0e}^2 \psi}{4P_e E_0 D_T l} \qquad (7)$$

$$\alpha_{min}^{PM} = \sqrt{\frac{h\nu_e}{\eta P_e}} \Delta f \frac{1}{l} \qquad (8)$$

Here, h is Planck constant, ν_e and ν_p are frequencies of the excitation and probe beams; η is the detector quantum yield; Δf is the detection channel bandwidth; ψ is chopper frequency in PT measurements; B_∞ is the steady-state geometry constant of the setup optical scheme, other parameters are listed above.

CBV assessment

We used dyes for intravenous administration for simultaneous PT and optical absorbance determination of components of their two-dye mixtures in circulating blood. CBV were measured as an average of two PT signals for each dye to decrease the interference of both dyes on one another and thus to improve the accuracy (and determined after their dilution in circulation. The concentration of each dye diminishes due to dilution. From the curve of the relative decrease in the concentration, CBV is calculated from the ratio of concentrations of the initial dye solution and the solution of dye in the blood according to the following equation [18-21]:

$$CBV = V_0\ \vartheta_0/\vartheta_x = V_0\ A_0/A_x = V_0\ c_0/c_x, \qquad (9)$$

where ϑ is PT signal amplitude, A is absorbance, V_0 and c_0 are initial volume and concentration of the dye solution, and c_x is the dye concentration in the blood after the dilution. The determination of two components a and b of a dual-component mixture was made using two methods (i) a standard Vierordt's method at two wavelengths λ_1 and λ_2 [22-24]:

$$\begin{cases} A^{\lambda_1} = l(c_a \varepsilon_a^{\lambda_1} + c_b \varepsilon_b^{\lambda_1}) \\ A^{\lambda_2} = l(c_a \varepsilon_a^{\lambda_2} + c_b \varepsilon_b^{\lambda_2}) \end{cases}. \qquad (10)$$

and (ii) using an overdetermined Vierordt's system at four wavelengths to decrease the overall error [22]:

$$\begin{cases} \Delta A_a = A^{\lambda_1} - A^{\lambda_2} = l[c_a(\varepsilon_a^{\lambda_1} - \varepsilon_a^{\lambda_2}) + c_b(\varepsilon_b^{\lambda_1} - \varepsilon_b^{\lambda_2})] \\ \Delta A_b = A^{\lambda_3} - A^{\lambda_4} = l[c_a(\varepsilon_a^{\lambda_3} - \varepsilon_a^{\lambda_4}) + c_b(\varepsilon_b^{\lambda_3} - \varepsilon_b^{\lambda_4})] \end{cases}. \qquad (11)$$

Here A is absorbance acquired from spectrophotometric measurements or calculated from PT measurements. The maxima of functions $\varepsilon_a^{\lambda_1}/\varepsilon_b^{\lambda_1} \sqrt{\varepsilon_a^{\lambda_1}\varepsilon_b^{\lambda_1}} = f(\lambda)$ and $\varepsilon_b^{\lambda_1}/\varepsilon_a^{\lambda_1} \sqrt{\varepsilon_a^{\lambda_1}\varepsilon_b^{\lambda_1}} = f(\lambda)$ were used as the wavelengths for Vierordt's method. For the overdetermined Vierordt's system (11), λ_1 and λ_3 were at the maxima, and λ_2 and λ_4 — at the minima of the absorption spectra of a and b components. The calculations of dye concentration were made taking into account the condition $c_a/c_b = $ const, which is correct for pre-prepared two-dye mixtures injected into the flow [22].

Reagents, solvents, and procedures

The following dyes were used Methylene Blue (MB, CAS no. 61-73-4), Brilliant Green (BG, CAS no. 633-03-4), Crystal Violet (CV, CAS no. 548-62-9), Indigo Carmine (CAS no. 860-22-0), and Bromsulphalein (CAS no. 71-67-0) and Evans Blue (CAS no. 314-13-6); their stock solutions of 0.10% wt. in PBS (20 mM, pH 7.4) were used throughout. Other reagents are high-purity 0.1 M KOH, conc. cp HNO3, and p.a. acetone. Water from a TW-600RU water purification system (Nomura MicroScience Co., Ltd.; Okada, Atsugi-City, Kanagawa, Japan) was used: pH 6.8; specific resistance 18.2 MΩ×cm, Fe, 2 ppt; dissolved SiO2, 3 ppb; total ion amount, < 0.2 ppb; TOC, < 10 ppb. Solutions were made using a Branson 1510 ultrasonic bath (USA), power 1 W (exposure times 10–15 min). The glassware was

washed with acetone followed by conc. nitric acid. The blood of rats stabilized with heparin was used at the stages of blood batch and flow tests.

Determination of label dyes under batch conditions

Stock solutions of selected dyes in blood (0.40 mL of the stock solution of the corresponding dye and 0.60 mL of blood) were used. This freshly prepared stock solution was diluted in the photometric cells by adding a 0.01 – 0.05 mL of this solution to 0.40 mL of blood. The calibrations were made at wavelengths 615, 630, 663, and 690 nm, and the limits of detection and other performance parameters were measured.

In vitro assessment of circulating blood volume

The main glass vessel of the manifold was filled with the precisely measured blood volume, and the blood started circulating through the manifold. When the regular flow through the cell is established, the zero absorbance is calibrated. Next, 0.4 mL of an aliquot of stock solutions of MB and CV or their mixture of was injected, and the absorbances at 615, 630, 663, and 690 nm was recorded until constant absorbance/PT value are reached. The concentrations of labels were determined from Eqs. (11).

Results and discussion

Back-synchronized spectrometer

We developed a PT-lens flow spectrometer working in batch and flow conditions using the available flow module and an absorption spectroscopy unit to real-time measure of absorption spectra of dye alone and in mixtures. In this excitation/data-treatment mode [3, 25], the advantages are (i) the possibility of detection under batch and flow conditions with no change in the optical-scheme design of the instrument; (ii) the possibility to switch between transient and steady-state thermal-lens measurements within a single set of experiments; and (iii) a wide linear dynamic range (more than five orders of magnitude of detectable absorbances) including strongly absorbing and scattering samples. In spite of a somewhat lower detection sensitivity compared to more commonly used lock-in detection schemes in thermal-lens spectrometry, the flexibility of this measurement mode provide a much larger volume of information, making it a powerful tool for solving so not-straightforward problems like studies of complex formation at trace concentrations, time-resolved heat dynamics around absorbing nanoparticles, etc. [22, 26-30].

The setup (Fig. 1) was made using the previously optimized schematics taking into account the precision of measurements and the linear range of thermal lens signal. The main idea is to combine photometric and PT measurements in a single setup. This idea was supported by our previous data on the use of the thermal-lens spectrometer as a single-wavelength photometer providing enough measurement precision [3].

The probe wavelength of 808 nm (marked grey in Fig. 1) was selected as it provided the minimum light absorption of the blood components according to our previous findings [31] and selected dyes and very low scattering. The probe intensity was attenuated to 1 mW at the output and ca. 0.7 mW at the cell. The excitation beam was made of four beams of diode lasers with the same beam parameters and the wavelengths of 610, 635, 660, and 690 nm. In a more advanced mode, the diode laser with the same beam parameters and the wavelength of 532 nm was added. The lasers are chopped in sequence synchronized with the main light chopper; thus, every excitation on–off cycle of the thermal lens corresponds to the certain wavelength, and the frequency of the excitation with the same wavelength is $\psi/4$ (or $\psi/5$ for a five-wavelength mode).

In order to get the maximum information for a flowing sample (at a flow rate of 35 mL/min), high chopper frequencies are preferable, while the sensitivity of PT measurements decrease with the chopper frequency [12]. Thus, a compromise frequency of 10 Hz was used, which corresponded to 2.5 Hz frequencies for a single wavelength. This corresponded to the measurement of *ca.* 0.15 mL of the flowing sample with a certain wavelength and 0.45 mL with other wavelengths, in cycles.

To implement dual-mode measurements, we used a dichroic mirror to separate the probe beam from the excitation. The whole excitation beam after the cell penetrated the dichroic mirror and was gathered with a focusing lens by the primary photometric detector, which was compared with pre-calibrated power meter used as the absorbance ground signal. The selection of the optimum parameters of PT measurements are discussed previously [3, 25].

Heme protein studies

The PT determination of some Hb species (desoxyhaemoglobin and oxyhaemoglobin shows the limits of detection at the level of 10^{-8} M as in the previous study [31] but with lower errors due to the use of multiple wavelengths.

The experiments with haemoglobin cyanide species with the back-synchronized measurement mode showed that the changes in amplitude and time-resolved thermal-lens signal can be used for determining the dispersity of the solution.

The determination of HbCN and ferroin selected as a highly absorbing chelate shows low and silmilar

LODs under the excitation conditions (Table 2). However, time-resolved curves for molecular and colloid solutions of HbCN differ (Fig. 2, a) and the characteristic time of thermal-lens measurements, Eq. (4), changes significantly (Table 2), while the slope of the calibration plot goes lower than expected. This is in contrast to ferroin, for which the calculated and experimental value are in good agreement. This behavior is due to faster heating of the vicinity of the absorbing disperse particles, which decreases the characteristic time and slower heat transfer into the solution body, which decreases the steady-state thermal lens signal. This model for thermal lensing in HbCN solutions is well simulated by the developed theoretical approach [8, 10].

Moreover, the overall change in t_c is additive (see Table 2 and Fig. 2, b): an equimolar mixture of HbCN and ferroin shows a expected change in the slope and a shift in the characteristic time. This, also can be predicted by the approach [8, 10] however, this requires further development in the theory.

The characteristic time of thermal lens in HbCN solutions depend on the concentration of the protein (Fig. 3). The dependence is described with the empirical equation

$$t_{c,disp} = k_1 t_{c,aq} - k_2 cd \qquad (12)$$

Here, $t_{c,disp}$ and $t_{c,aq}$ are thermal lens characteristic times for a test disperse system and water, c is disperse particle molarity, d is their average diameter and k_1 and k_2 are empiric coefficients. From this dependence, the size of hemoglobin cyanide molecule, (6.0 ± 3.0) nm was calculated the developed approach for heterogonous systems in TLS. This value is in good agreement with the size of the hemoglobin globule [32].

Table. 2. Performance parameters and characteristic times of thermal-lens determination of ferroin as a molecular chelate dye and hemoglobin cyanide under various conditions in a phosphate buffer solution, pH 7.0 and in a highly saline solution ($P = 0.95$, $n = 6$), $\lambda = 532$ nm, excitation power 47.5 mW

Substance	LOD,	Calibration slope	t_c, ms
Calculated (PBS)	—	5.20	6.3
Ferroin, PBS	60	5.2 ± 0.1	6.2 ± 0.1
HbCN, PBS	30	3.26 ± 0.09	4.8 ± 0.2
Ferroin : HbCN 1 :1	—	5.5 ± 0.1	5.3 ± 0.2
Calculated (saline)	—	5.22	6.1
Saline ferroin	60	5.2 ± 0.1	6.0 ± 0.2
Saline HbCN	20	5.8 ± 0.1	6.0 ± 0.2

Saline = 0.4M KCl + 2.8M NaCl; LOD is in nmol/L
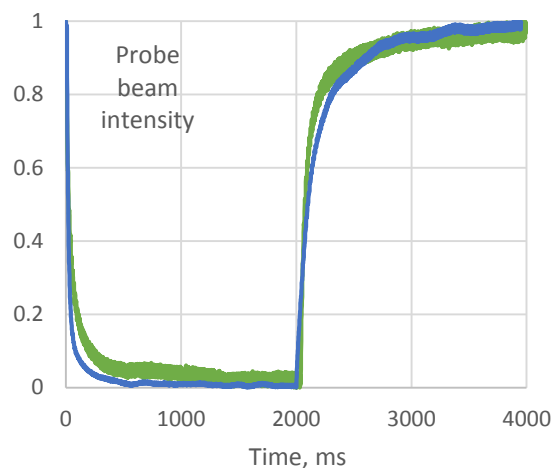
a
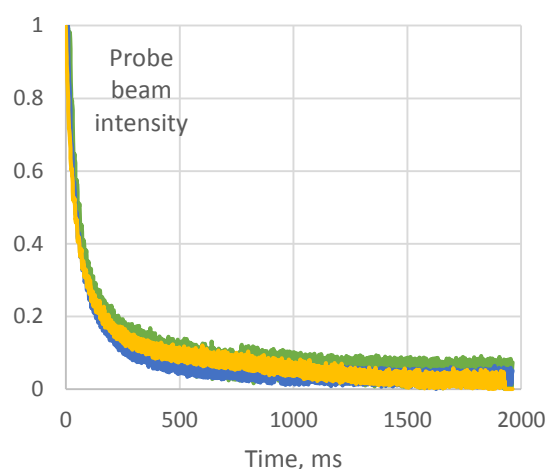
b

Fig. 2. Transient curves of thermal-lens signals from for a molecular dye (ferroin), green line, and hemoglobin cyanide, blue line, with the same absorbance. (a) are full curves for pure substances; (b) are thermal-lens development curves only with the yellow line corresponding to 1 : 1 molar mixture of ferroin and hemoglobin cyanide), $\lambda = 532$ nm, excitation power 47.5 mW
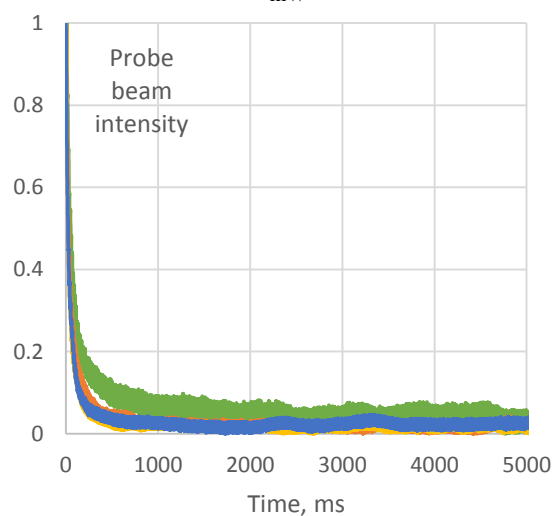

Fig. 3. Transient thermal-lens development curves of thermal-lens signals from for haemoglobin cyanide in PBS (2×10^{-7} M, green line, 8×10^{-7} M, orange line, 1.5×10^{-6} M, blue line, and 3×10^{-7} M, yellow line)), $\lambda = 532$ nm, excitation power 47.5 mW.
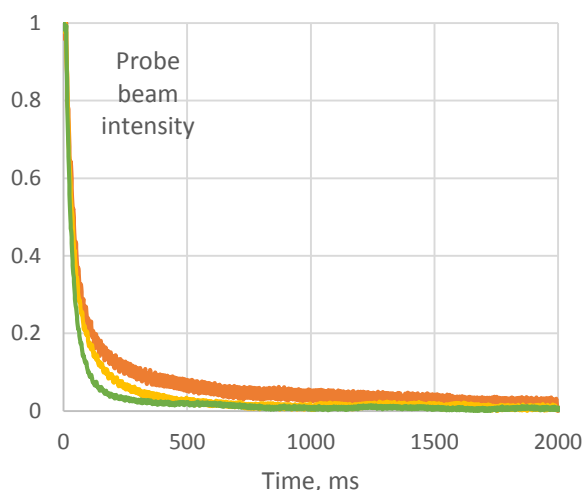
Fig. 4. Transient thermal-lens development curves of thermal-lens signals from for a hemoglobin cyanide in PBS (green line) 3M NaCl (yellow line) and in 5 M NaClO$_4$ (orange line) , λ = 532 nm, excitation power 47.5 mW.

Moreover, this change in the shape of transient thermal-lens curves makes it possible to estimate the state of these proteins in solution. For hemoglobins, an increase in the ionic strength from (i) standard phosphate buffers to highly saline (ii) NaCl, and (iii) NaClO$_4$ solutions results in the ratio of the TLS signal amplitudes as i : ii : iii of 1 : 2 : 4, which is in good concordance with the existing data [33] for the decomposition of hemoglobin into 2 and 4 subunits, respectively. Measuring the model molecular dye (ferroin) and HbCN under these conditions shows the number of changes. The characteristic times of transient curves and calibration slopes for ferroin do not change as expected (Table 2). To the contrary, the curve for hemoglobin in NaCl start to go much closer to the curve of ferroin (Fig. 4) and t_c differ much less significantly (Table 2) due to dissociation of tetramers to dimers; and in NaClO$_4$ solutions the transient curve for HbCN start to differ insignificantly from the ferroin solution due to final dissociation to monomers [33].

PT-lens measurements of the circulating blood volume

The ability of thermal-lensing to change sensitivity in protein solutions was used in the measurement of circulating blood volume (**CBV**) by the designed setup. CBV is crucial in various medical conditions including surgery, iatrogenic problems, rapid fluid administration, transfusion of red blood cells, or trauma with extensive blood loss including battlefield injuries and other emergency situations loss [18, 20, 34-37]. Currently available commercial techniques are invasive and time-consuming for trauma situations [35, 36]. Recently, we have proposed high-speed multi-wavelength photoacoustic/photothermal (PA/PT) flow cytometry for *in vivo* CBV assessment with multiple dyes as PA and PT contrast agents (labels) [22].

Photothermal vs. photometric sensitivity comparison

According to Eq. (13), it is possible to compare the sensitivity of photometric and PT measurements and for the same detector and the same laser used for measuring absorption and PT excitation. The comparison of sensitivities for the same detector type (η and Δf parameters in eq. (7)) and the same source of absorption/PT excitation is given by the equation deduced from (7) and (8)

$$\alpha_{min}^{PT}/\alpha_{min}^{PM} = \sqrt{\frac{2\nu_p}{\nu_e P_e P_p}}\; \frac{\omega_0^2 \psi}{4E_0 D_T} =$$
$$= \sqrt{\frac{2\lambda_e}{\lambda_p P_p}}\; \frac{B_\infty \omega_0^2 \psi}{4E_0 D_T}\; \frac{1}{\sqrt{P_e}} \tag{13}$$

This equation shows that an increase in the sensitivity depends on the geometry parameters of the setup and the parameters of the medium, in which the thermal lens is bloomed. For the experimental conditions discussed above the calculation shows that the minimum detectable linear absorption coefficient is about 250-fold lower that for photometry. This means that the significant diminishing of dye doses to get reliable PT signals compared to current clinical doses (for PDD, 2.5–5 mg/mL) can be made when shifting from optical photometric to PT measurements of CBV.

Photothermal measurements of model dyes in blood

As additional verification of our proof-of-concept of the PT part of this technique, here we performed optical photometric and PT CBV measurements *in vitro* with the described above multi-wavelength photothermal-lens spectrometer. Two label dyes—Methylene Blue and Crystal Violet—were selected for simultaneous photometric/PT determination of the components of their two-dye mixtures in the circulating blood *in vitro*. Working concentrations of both label dyes, MB and CV were diminished by a factor of *ca.* 50 compared to existing CBV methods and to the level used for optical photometric measurements in his study to 10 nmol/l. From absorption spectra, the linear absorption coefficient for MB and CV in blood at the selected wavelengths at the red region are 20–25 cm^{-1} at 100 μM (0.1 mg/mL) while blood absorption at IR laser line of 808 nm is 4–5 cm^{-1} at 808 nm [38, 39]. The examples of flow measurements of both dyes by PT spectrometry are shown in Fig. 5.

The minimum delectable concentrations of MB and CV in blood by PT measurements under the selected conditions are 0.2 and 0.5 μM, respectively which is 250 times lower than the clinically approved doses [39]. These values are in good agreement with the theoretical estimations from Eq. discussed in the previous section. The estimations of CBV assessment in the test manifold showed the error of assessment is below 5% for blood volumes 0.3–5 L and above concentrations of dyes diminished

compared to photometric measurements. The error of measurements agrees well with our previous data on PA measurements of blood parameters [22, 40].
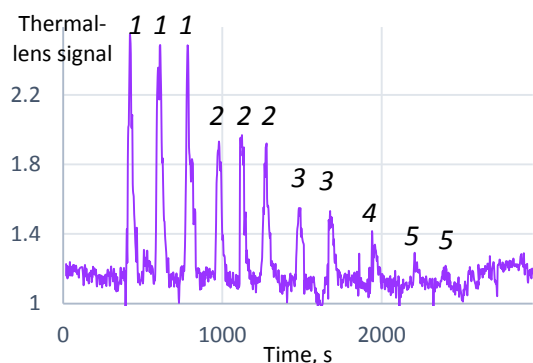

Fig. 5. Dilution curves for photothermal measurements of Crystal Violet. Concentrations: (*1*, 1.2×10^{-4} M; *2*, 6.5×10^{-5} M; *3*, 3.3×10^{-5} M; *4*, 1.6×10^{-5} M; *5*, 1.1×10^{-5} M.

Conclusions

Thermal lens spectrometry can be implemented as a multifunctional device for various fundamental and applied studies on heme proteins and their solutions. This thermal-lens approach can be used for determining state-of-the-art nanomaterials like nanodiamond and fullerenes, which are not considered within the frames of this study. Also, the transient thermal lensing can be used to overcome the diffraction limit of optical photothermal spectroscopy to attain super-resolution of photothermal imaging, which is of high importance for various applications like studies of mitochondria, erythrocyte pathologies and similar problems [41, 42]. The following studies should be focused on the integration of all the modes of photothermal measurements in a single compact device for micro-measurements [2].

Acknowledgements

References

[1] M.A. Proskurnin and M.Y. Kononets (2004), Modern analytical thermooptical spectroscopy, Uspekhi Khimii, 73, 1235-1268.
[2] T. Yamamoto, Y. Kazoe, K. Mawatari and T. Kitamori (2011), Micro and nano chemical systems, Journal of Synthetic Organic Chemistry Japan, 69, 526-533.
[3] M.A. Proskurnin, A.G. Abroskin and D.Y. Radushkevich (1999), A dual-beam thermal lens spectrometer for flow analysis, J. Anal. Chem. (Russ.), 54, 91-97.
[4] K.A. Ghaleb and J. Georges (2004), Photothermal spectrometry for detection in miniaturized systems: Relevant features, strategies and recent applications, Spectrochimica Acta Part a-Molecular and Biomolecular Spectroscopy, 60, 2793-2801.
[5] J. Shen, R.D. Lowe and R.D. Snook (1992), A model for cw laser-induced mode-mismatched dual-beam thermal lens spectrometry, Chemical Physics, 165, 385-396.
[6] J. Shen, A.J. Soroka and R.D. Snook (1995), Model for cw laser-induced mode-mismatched dual-beam thermal lens spectrometry based on probe beam profile image detection, Journal of Applied Physics, 78, 700-708.
[7] R.D. Snook and R.D. Lowe (1995), Thermal lens spectrometry - a review, Analyst, 120, 2051-2068.
[8] D.A. Nedosekin, M.A. Proskurnin and M.Y. Kononets (2005), Model for continuous-wave laser-induced thermal lens spectrometry of optically transparent surface-absorbing solids, Applied Optics, 44, 6296-6306.
[9] D.A. Nedosekin, A.V. Pirogov, W. Faubel, U. Pyell and M.A. Proskurnin (2006), Investigation of ionene adsorption on quartz surfaces by thermal-lens spectrometry, Talanta, 68, 1474-1481.
[10] A.V. Brusnichkin, D.A. Nedosekin, M.A. Proskurnin and V.P. Zharov (2007), Photothermal lens detection of gold nanoparticles: Theory and experiments, Applied Spectroscopy, 61, 1191-1201.
[11] D.A. Nedosekin, M.Y. Kononets, M.A. Proskurnin, T.Y. Chaikovskii and G.V. Lisichkin (2007), Potential of thermo-optical methods for the study of molecular layers bonded to a flat glass surface, J. Anal. Chem. (Russ.), 62, 126-135.
[12] A. Smirnova, M.A. Proskurnin, S.N. Bendrysheva, D.A. Nedosekin, A. Hibara and T. Kitamori (2008), Thermooptical detection in microchips: From macro- to micro-scale with enhanced analytical parameters, Electrophoresis, 29, 2741-2753.
[13] D.A. Nedosekin, W. Faubel, M.A. Proskurnin and U. Pyell (2009), Determination of light-absorbing layers at inner capillary surface by cw excitation crossed-beam thermal-lens spectrometry, Talanta, 78, 682-690.
[14] D.A. Nedosekin, W. Faubel, M.A. Proskurnin and U. Pyell (2009), Sensitivity enhancement of thermal-lens spectrometry using laser-induced precipitation, Analytical Sciences, 25, 611-616.
[15] D.A. Nedosekin, W. Faubel, M.A. Proskurnin and U. Pyell (2009), Determination of light-absorbing layers at inner capillary surface by cw excitation crossed-beam thermal-lens spectrometry, Talanta, 78, 682-690.

[16] A.V. Brusnichkin et al (2010), Ultrasensitive label-free photothermal imaging, spectral identification, and quantification of cytochrome c in mitochondria, live cells, and solutions, Journal of Biophotonics, 3, 791-806.

[17] A.Y. Luk'yanov, G.B. Vladykin, M.A. Novikov and Y.I. Yashin (1999)Journal of Analytical Chemistry, 54.

[18] D.M. Takanishi, Jr. et al (2009), The availability of circulating blood volume values alters fluid management in critically ill surgical patients, Am J Surg, 197, 232-237.

[19] O.A. Kovalev and V.N. Grishanov (1976), [determination of the volume of circulating blood by using evans blue dye], Lab Delo, 664-667.

[20] S. Henschen, M.W. Busse, S. Zisowsky and B. Panning (1993), Determination of plasma volume and total blood volume using indocyanine green: A short review, J Med, 24, 10-27.

[21] A.A. Riley, Y. Arakawa, S. Worley, B.W. Duncan and K. Fukamachi (2010), Circulating blood volumes: A review of measurement techniques and a meta-analysis in children, ASAIO J, 56, 260-264.

[22] M.A. Proskurnin et al (2011), In vivo multispectral photoacoustic and photothermal flow cytometry with multicolor dyes: A potential for real-time assessment of circulation, dye-cell interaction, and blood volume, Cytometry Part A, 79A, 834-847.

[23] J. Karpinska, A. Sokol and M. Rozko (2009), Applicability of derivative spectrophotometry, bivariate calibration algorithm, and the vierordt method for simultaneous determination of ranitidine and amoxicillin in their binary mixtures, Anal Lett, 42, 1203-1218.

[24] E. Dinc and F. Onur (1997), Comparative study of the ratio spectra derivative spectrophotometry, derivative spectrophotometry and vierordt's method applied to the analysis of oxfendazole and oxyclozanide in a veterinary formulation, Analusis, 25, 55-59.

[25] M.A. Proskurnin and A.G. Abroskin (1999), Optimization of optical system parameters in dual-beam thermal lens spectrometry, J. Anal. Chem. (Russ.), 54, 401-408.

[26] D.S. Tsar'kov, E.S. Ryndina, M.A. Proskurnin and V.M. Shkinev (2011), Extraction-thermal lens quantification of cobalt with nitroso-r-salt in two-phase aqueous systems with water-soluble polymer polyethylene glycol, J. Anal. Chem. (Russ.), 66, 166-170.

[27] N.V. Saranchina, A.V. Sukhanov, D.A. Nedosekin, N.A. Gavrilenko and M.A. Proskurnin (2011), Potentials of thermal lens spectroscopy for polymethacrylate optical sensors, J. Anal. Chem. (Russ.), 66, 623-628.

[28] M.A. Proskurnin, E.S. Ryndina, D.S. Tsar'kov, V.M. Shkinev, A. Smirnova and A. Hibara (2011), Comparison of performance parameters of photothermal procedures in homogeneous and heterogeneous systems, Analytical Sciences, 27, 381-387.

[29] M.A. Proskurnin, E.V. Ageeva, A.A. Shelepchikov and V.V. Senyuta (2010), Use of poorly absorbing materials and low-contrast photometric reactions in thermal lens spectrometry, J. Anal. Chem. (Russ.), 65, 713-725.

[30] D.A. Nedosekin, A.V. Brusnichkin, A.Y. Luk'yanov, S.A. Eremin and M.A. Proskurnin (2010), Heterogeneous thermal-lens immunoassay for small organic compounds: Determination of 4-aminophenol, Applied Spectroscopy, 64, 942-948.

[31] A. Brusnichkin et al (2009), Determination of various hemoglobin species with thermal-lens spectrometry, Moscow University Chemistry Bulletin, 64, 45-54.

[32] M. Paoli, R. Liddington, J. Tame, A. Wilkinson and G. Dodson (1996), Crystal structure of t state haemoglobin with oxygen bound at all four haems, Journal of Molecular Biology, 256, 775-792.

[33] G. Guidotti (1967), Studies on the chemistry of hemoglobin: Ii. The effect of salts on the dissociation of hemoglobin into subunits, Journal of Biological Chemistry, 242, 3685-3693.

[34] A. Lozhkin, T. Makedonskaya, G. Pakhomova and O. Loran (2010), Estimation of the trauma severity degree in injured with associated injuries depending on the blood loss, Vox Sang, 99, 435-436.

[35] W. Baulig, E.O. Bernhard, D. Bettex, D. Schmidlin and E.R. Schmid (2005), Cardiac output measurement by pulse dye densitometry in cardiac surgery, Anaesthesia, 60, 968-973.

[36] M. Kroon, A.B. Groeneveld and Y.M. Smulders (2005), Cardiac output measurement by pulse dye densitometry: Comparison with pulmonary artery thermodilution in post-cardiac surgery patients, J Clin Monit Comput, 19, 395-399.

[37] L. Donner and V. Maly (1955), [total blood volume in some blood diseases. Ii. Results in pernicious anemia, anemia following hemorrhage, polycythemia vera, secondary polyglobulia and leukemia.], Sb Lek, 57, 125-136.

[38] G. Ku and L.V. Wang (2005), Deeply penetrating photoacoustic tomography in biological tissues enhanced with an optical contrast agent, Opt Lett, 30, 507-509.

[39] X. Wei, J.M. Runnels and C.P. Lin (2003), Selective uptake of indocyanine green by reticulocytes in circulation, Invest Ophthalmol Vis Sci, 44, 4489-4496.

[40] E.I. Galanzha and V.P. Zharov (2011), In vivo photoacoustic and photothermal cytometry for monitoring multiple blood rheology parameters, Cytometry Part A, 79A, 746-757.

[41] D.A. Nedosekin et al (2012), Synergy of photoacoustic and fluorescence flow cytometry of circulating cells with negative and positive contrasts, J Biophotonics.

[42] D.A. Nedosekin, E.V. Shashkov, E.I. Galanzha, L. Hennings and V.P. Zharov (2010), Photothermal multispectral image cytometry for quantitative histology of nanoparticles and micrometastasis in intact, stained and selectively burned tissues, Cytometry Part A, 77A, 1049-1058.